# Ultrafast Thermal Analysis of Surface Functionalized Gold Nanorods in Aqueous Solution

Jingyu Huang,[†] Jonglo Park,[‡] Wei Wang,[‡] Catherine J. Murphy,[†,*] and David G. Cahill[‡,*]

[†]Department of Chemistry, University of Illinois at Urbana—Champaign, Urbana, Illinois 61801, United States and [‡]Department of Materials Science and Engineering, and Materials Research Laboratory, University of Illinois at Urbana—Champaign, Urbana, Illinois 61801, United States

ABSTRACT The thermal conductivity and heat capacity of surfactant and polyelectrolyte coatings of gold nanorods (GNRs) in aqueous solution are investigated by transient absorption, following femtosecond pumping of the longitudinal localized surface plasmons. Surfactant and polyelectrolyte layer thicknesses are measured by dynamic light scattering (DLS). The GNRs are initially coated with a bilayer of the quaternary ammonium surfactant cetyltrimethylammonium bromide (CTAB). The rate of change of the absorption of gold nanorods in aqueous solution varies with the probe laser wavelength due to the shift in the plasmon resonance created by heating of media around the particles. The cooling dynamics of gold nanorods are best measured by tuning the pump—probe laser wavelength to the absorption peak of the sample. The heat capacity of the surfactant layer is 2.0 ± 0.3 J cm^{-3} K^{-1}; the thermal conductivity of the surfactant layer drops from 0.24 to 0.18 W m^{-1} K^{-1} at solution concentrations above the CTAB critical micelle concentration (cmc). Layer-by-layer polyelectrolyte coatings using poly(acrylic acid) (PAA) and polyallyamine hydrochloride (PAH) increase the thermal conductivity and heat capacity of the surface layer. PAH-terminated layers have increased thickness, thermal conductivity, and heat capacity relative to PAA-terminated layers; this effect is attributed to greater water penetration into PAH-terminated surface layers.
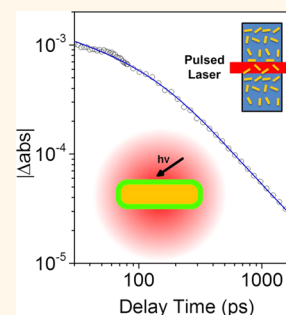
KEYWORDS: gold nanorod · nanoscale thermal transport · transient absorption · femtosecond pulsed laser · cetyltrimethylammonium bromide · polyelectrolyte layer-by-layer coating

G old nanorods (GNRs) exhibit both transverse and longitudinal surface plasmon resonances, tunable from the visible to the near-infrared (NIR) as a function of nanorod shape,[1,2] and can absorb photons and convert light into heat through a series of nonradiative photophysical processes.[3] That light can be converted into sufficient heat to, for example, kill cancer cells, has sparked enormous interest in the nanomedicine community: it is a rare example of a nanoparticle being "active" as a therapeutic rather than a passive deliverer of drug molecules.[3] When a gold nanorod interacts with a femtosecond laser pulse, the photothermal events include (1) an increase in the electron temperature, through electron—electron scattering, within several hundred fs; (2) an increase in the lattice temperature, through electron—phonon coupling, within 1—10 ps; (3) dissipation of heat from the hot particle to the surrounding media to reach thermal equilibrium within 100 ps to several ns, depending on

the particle size, thermal properties of the surroundings, and laser intensity.[3−5]

The combination of photothermal effects with the ability to functionalize the GNR surface has led to potential biological applications of GNRs such as targeted cell ablation[6−8] and targeted drug delivery.[9−12] Engineering applications of GNRs and other plasmonic nanomaterials require improved scientific understanding of thermal transport at the nanocale.[13,14] For example, understanding how, and how fast, heat is dissipated from nanoparticles is important for not only photothermal therapies, but also for using plasmon-induced heat to promote new and improved chemical reactions.[15−18] Moreover, the study of thermal transport can provide information about vibrational energy transfer through molecular adsorbates, and thereby probe the properties of the adsorbed molecular layer.[19,20]
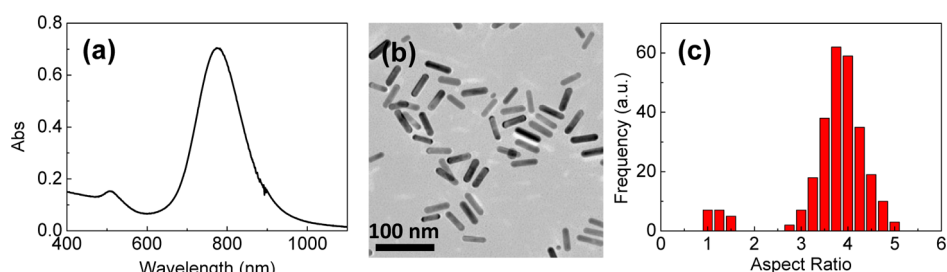
Pump—probe transient absorption has been widely applied to study heat transfer

Figure 1. (a) UV−vis absorption spectrum of GNRs in aqueous solution. (b) Transmission electron micrograph (TEM) of the GNRs; the scale bar is 100 nm. (c) Distribution of the aspect ratios of GNRs as measured from TEM micrographs.

from noble metal nanoparticles to their surroundings.[21−27] The particle/water interface thermal conductance (G) of GNRs with different ligands on their surface has been studied by Hamad-Schifferli et al. by probing absorption changes in the longitudinal surface plasmon band; these transient absorption changes were modeled numerically to extract values for the effective interface thermal conductance G.[24,25] However, in their work[24,25] the model fitting could only be applied to absorption changes at time scales longer than 300 ps, and their calculated thermal conductivity (the product of G and thickness of the ligand layer) of the surface layers were ∼1 W m^{-1} K^{-1}, much larger than the typical values of 0.1−0.5 W m^{-1} K^{-1} for organic materials.[28] Hamad-Schifferli et al. used a frequency-doubled pump laser at 400 nm to heat the GNRs (which had a longitudinal plasmon peak at 770 nm) and a probe laser at 800 nm to perform the transient absorption experiments. Transient absorption data taken at the red side of the plasmon band will include contributions from both gold nanorod cooling and the heating of the surrounding media;[26,29] the sum of these two processes can be misinterpreted as large G values.

This artifact can be avoided by tuning the pump and the probe to the wavelength of peak absorption.[26,29] By combining transient absorption measurements at the wavelength of peak absorption and measurements of the coating thickness by dynamic light scattering (DLS), we find that we can determine both the thermal conductivity and heat capacity per unit volume of the nanorod coatings. Our approach for thermal analysis using temperature excursions on picosecond to nanosecond time-scales is analogous to the use of the plasmon resonance to probe the index of refraction of the immediate surroundings of the nanorods. The plasmon resonance involves electric fields that are localized to the close proximity of the nanorod. Following rapid heating of the nanoparticle by the pump optical pulse, temperature excursions are similarly confined on small length scales. Thermal diffusion constants in water or organic layers are on the order of 10^{-3} cm^2 s^{-1}. Therefore, thermal diffusion distances on time-scales of 10 ps to 1 ns are 2 to 20 nm, which are the thicknesses of the layers in our experiments.

RESULTS AND DISCUSSION

Gold nanorods were prepared by the aqueous seed-mediated and silver-assisted method.[30] The aspect ratio was controlled so that the longitudinal surface plasmon wavelength maximum was at ∼776 nm. Transmission electron microscopy (TEM) showed that the GNRs had average dimensions 46 ± 5 nm ×12 ± 1.1 nm, for an aspect ratio of 3.8 (Figure 1). ζ-Potential measurements confirmed that the GNR colloids were positively charged at pH 7, due to the cationic surfactant cetyltrimethylammonium bromide (CTAB) bilayer on the surface of the synthesized GNRs.[1,31] Data regarding the CTAB bilayer comes from thermogravimetric and FTIR data, which provide no information about the homogeneity of the overall surface coating; we assume uniform coverage as a reasonable starting point.[31] GNR concentrations in aqueous solution were kept at ∼0.15 nM for absorption spectra measurements and ∼1 nM for transient absorption and dynamic light scattering measurements. The optical path length of the sample solutions was 1 cm for absorption spectra measurements and 0.1 mm for transient absorption measurements.

Transient absorption was used to probe thermal transport from the GNR, through the organic coatings, and into the surrounding water. A laser power of 1.5 mW was chosen for both pump and probe beams compromise between a high level of signal-to-noise and low temperature rise of the GNRs. The average transient heating for the entire ensemble GNRs was estimated to be 7 K by dividing the total energy absorbed by the GNRs per pump laser pulse with the volumetric heat capacity of gold and the total volume of gold in the laser beam spot. The temperature excursions of individual GNRs vary widely because of the dependence of the optical cross-section on orientation and aspect ratio. We estimate a maximum heating of 45 K for GNRs with the maximum optical cross-section. For such temperature rises, there should be no nanorod melting or shape change;[3,32] the observation of stable signals upon repeated transient absorption experiments at the same sample spot also suggests that GNRs are stable under this laser power. Transmission electron micrographs of GNRs before and after such laser illumination show no change in overall
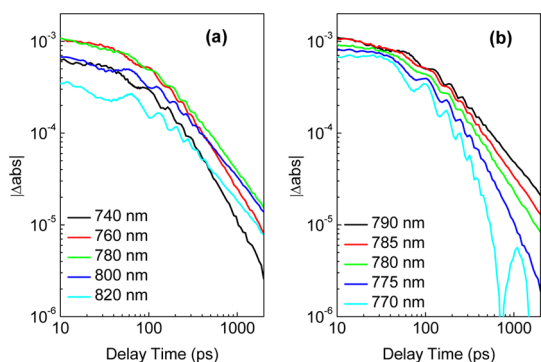
Figure 2. (a) Transient absorption of CTAB-coated GNRs in aqueous solution as a function of pump and probe wavelength, changed simultaneously. (b) Transient absorption of CTAB-coated GNRs in aqueous solution by fixing the pump wavelength at 790 nm and changing the probe wavelength from 790 to 770 nm. For the data at 770 nm, the transient absorption signal changes sign at a delay time of ∼700 ps.

particle size or shape. The absorbance change created by pump heating, $\sim 10^{-3}$, is small compared to the total absorbance of the sample solution of ~ 0.1. For such small absorbance excursions, the GNR absorbance can be considered to change linearly with the GNR temperature.[22,23]

To gain insight on how the transient absorption signal changes with the choice of pump and probe wavelengths, we first studied the transient absorption of the GNR aqueous solution using the same wavelength for the pump and probe and varied the wavelength from 740 to 820 nm, that is, from the blue side to the red side of the peak of the longitudinal plasmon absorption. The decay of the transient signal is faster at the blue side of the plasmon peak and slower at the red side (Figure 2a).

We also performed experiments using sharp edged optical filters[33] to fix the pump beam wavelength at 790 nm while changing the probe beam wavelength from 790 to 770 nm. (The homogeneous line-width of a single GNR of aspect ratio 3.8 is expected to be 30−40 nm[34] and therefore the absorption of our samples, see Figure 1a, has significant inhomogeneous broadening.) Using this approach, we observe an even more pronounced dependence of the decay of transient absorption on probe wavelength (Figure 2b) than when both the pump and probe wavelengths are changed simultaneously (Figure 2a).

The dependence of the transient absorption signal on the laser wavelength can be attributed to the effects of heating and resulting changes in the index of refraction of the surrounding media, when the heat flows out of GNR to the surroundings. The absorption spectra for ellipsoidal particles is described by the Gans theory:[3,5]

$$\sigma_{abs} = \frac{2\pi V}{3\lambda} \varepsilon_m^{3/2} \sum_{j=a,b,c} \frac{(1/P_j^2)\varepsilon_2}{(\varepsilon_1+(1-P_j)\varepsilon_m/P_j)^2+\varepsilon_2^2} \quad (1)$$

where σ_{abs} is the absorption cross section, V is the volume of the particle, λ is the wavelength of light, ε_m is the media dielectric constant, and ε_1 and ε_2 are the real and imaginary parts of gold dielectric constant, respectively. The depolarization factors P_j are defined by

$$P_a = \left(\frac{1-e^2}{e^2}\right)\left\{\frac{1}{2e}\ln\left(\frac{1+e}{1-e}\right)-1\right\} \quad (2)$$

$$P_b = P_c = \frac{1-P_a}{2} \quad (3)$$

where a, b, and c are the three axes of the nanoparticle, $a > b = c$, $e = (1-(1/AR)^2)^{1/2}$, and AR is the aspect ratio of the GNRs. Thus, the absorption spectra change of GNRs can be affected by both the dielectric constants of gold and the surrounding media. The total absorption cross section change can be considered to be the addition of both factors:[26]

$$\Delta\sigma_{abs}(\lambda) = \left(\frac{\partial\sigma_{abs}}{\partial\varepsilon_1}\frac{d\varepsilon_1}{dT_p}+\frac{\partial\sigma_{abs}}{\partial\varepsilon_2}\frac{d\varepsilon_2}{dT_p}\right)_\lambda \Delta T_p + \left(\frac{\partial\sigma_{abs}}{\partial\varepsilon_m}\frac{d\varepsilon_m}{dT_m}\right)_\lambda \Delta T_m \quad (4)$$

where T_p is the temperature of the gold nanorod, T_m is the temperature of the media surrounding the GNRs. Using Gans theory and the temperature-dependent optical properties of Au,[35] we estimate that the values of the six coefficients at the GNR plasmon absorption peak are $\partial\sigma_{abs}/\partial\varepsilon_1 \approx -2\times10^3$ nm^2; $\partial\sigma_{abs}/\partial\varepsilon_2 \approx -5\times10^3$ nm^2; $\partial\sigma_{abs}/\partial\varepsilon_m \approx -4\times10^2$ nm^2; $d\varepsilon_1/dT_p \approx 2\times10^{-3}$ K^{-1}; $d\varepsilon_2/dT_p \approx 2\times10^{-3}$ K^{-1}; $d\varepsilon_m/dT_m \approx -2\times10^{-4}$ K^{-1}.

Increasing the temperature of gold nanorods induces a red shift of the plasmon peak and a decrease in the peak height,[36−38] while the heating of water causes the water dielectric constant to decrease,[39] which blue-shifts the plasmon peak.[38,40] At short time scales, when the heat generated within the GNR has not yet been transferred to the surrounding media, ε_m is constant and the transient absorption signal is only due to the temperature increase of the GNRs; at long time scales when the heat has been transferred to the surrounding media, ε_m decreases and shifts the GNR absorption peak to blue. At the wavelength of peak absorption, the coefficient of the ΔT_p term in eq 4 is ≈ -14 nm^2 K^{-1}, while the coefficient of the ΔT_m term in eq 4 is close to zero, ~ 0.08 nm^2 K^{-1}. Thus, all subsequent measurements were performed by setting the wavelength of the pump and probe at the wavelength of peak absorption. These ensemble measurements collect data from nanorods with plasmon band maxima that are not exactly at the laser wavelength, since there is a variation in the aspect ratio in real samples; but to a good first approximation, shifts in the plasmon band as a function of temperature for higher and lower aspect ratio GNRs cancel each other out.
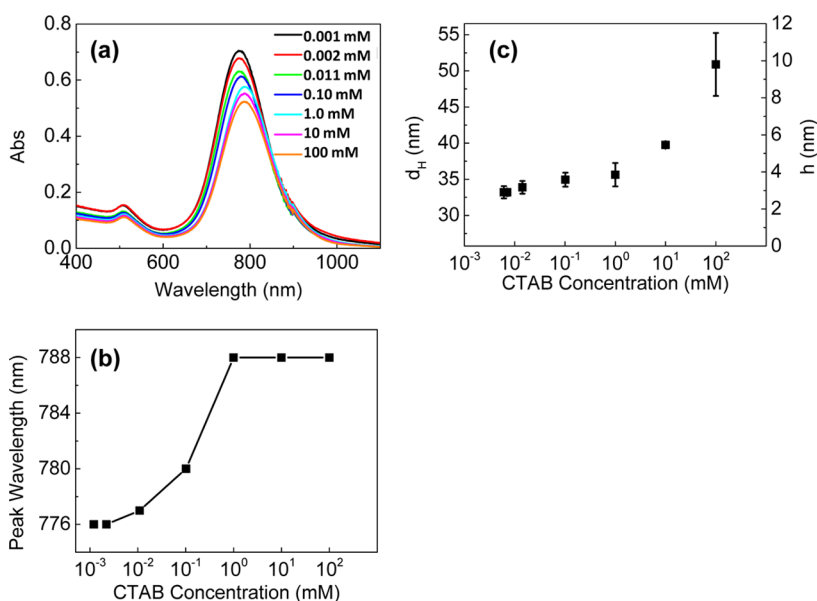
Figure 3. (a) UV−vis absorption spectra of ∼0.15 nM GNRs in CTAB solutions with different estimated final CTAB concentrations. (b) Longitudinal plasmon peak maxima for ∼0.15 nM GNRs in CTAB solutions as a function of the estimated final CTAB concentrations in the solutions. (c) Effective hydrodynamic diameters (d_H) of ∼1 nM GNRs in CTAB solutions measured by dynamic light scattering and equivalent thicknesses of CTAB bilayers (h) calculated from eqs 5−9 as a function of the estimated final CTAB concentrations in the solutions.

As-synthesized GNRs bear a bilayer of CTAB on their surfaces,[1,31] which is in equilibrium with free CTAB in solution. (The fact that other quaternary ammonium surfactants can exchange with CTAB upon prolonged exposure[41] provides evidence that the kinetics are sufficient to establish equilibrium between the bound nanorod coating and that free in the solution.) To vary the properties of the CTAB surface layer, GNR pellets were dispersed in CTAB solutions with the concentration varying from 0 to 100 mM. The final CTAB concentration in the sample solution was estimated with the assumptions that (1) the GNRs originally had a 3.9 nm CTAB layer before dispersion, and after dispersion, part of the CTAB molecules originally on the GNR surface desorb and reduce the CTAB layer thickness to what has been estimated from DLS data, see the discussion below; and (2) the CTAB layer has a density of 1 g mL^{-1}. The final CTAB concentration in the sample solution is the sum of the starting CTAB concentration in the solution and the contribution from CTAB removed from the GNR surface (Figure 3b,c), which also depends on the GNR concentration in the sample solution.

The plasmon peak of the sample shifted to the red, from 776 to 788 nm (Figure 3a,b) as the CTAB solution concentration increased from 0.001 mM to the critical micelle concentration (cmc), 0.92−1.00 mM.[42,43] As expected, the wavelength of peak absorption stayed constant at concentrations exceeding the cmc since the presence of CTAB micelles in solution approximately fixes the chemical potential.

Dynamic light scattering measurements showed a small increase of the effective hydrodynamic diameter (d_H) of the GNRs in water upon an increase in the CTAB solution concentration up to 1 mM CTAB in solution (Figure 3c). From 1 to 100 mM, the apparent size of all objects in solution increases much more dramatically, an effect that we attribute to the presence of CTAB micelles in the solution. The experimental thickness (h) of the CTAB bilayer can be extracted from the hydrodynamic diameters using the following relationships:[44,45]

$$d_H = \frac{k_B T}{3\pi\eta D_t} \tag{5}$$

$$D_t = \frac{k_B T \ln(L/d_{cs}) + C_t}{3\pi\eta L} \tag{6}$$

$$C_t = 0.312 + 0.565\left(\frac{d_{cs}}{L}\right) - 0.100\left(\frac{d_{cs}}{L}\right)^2 \tag{7}$$

$$L = L_{GNR} + h \tag{8}$$

$$d_{cs} = d_{GNR} + h \tag{9}$$

where d_H is the hydrodynamic diameter due to the translational diffusion of the GNRs, k_B is the Boltzmann constant, T is the temperature of sample solution, η is the solution viscosity, D_t is the translational diffusion constant, L is the total length of the coated GNR, d_{cs} is the total diameter of the coated GNR, L_{GNR} and d_{GNR} are the bare average length and diameter of the GNRs measured from TEM micrographs. As these DLS measurements are made over long time scales compared to the transient optical experiments, the thickness estimate of the layers necessarily assumes a constant
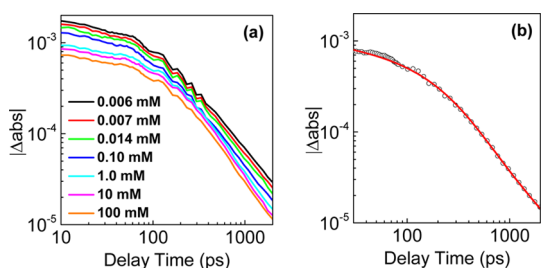
Figure 4. (a) Transient absorption of GNRs in CTAB solutions with different estimated final CTAB concentrations. (b) Circles: raw data of GNRs in 1 mM CTAB solution from pump−probe measurement; line: fitting for thermal conductivity of 0.18 W m^{-1} K^{-1} and volumetric heat capacity of 2.0 J cm^{-3} K^{-1} for the CTAB bilayer.

TABLE 1. Thickness of CTAB Layers on GNRs in CTAB Solutions with Different Estimated Final CTAB Concentrations

[CTAB] (mM)	0.006	0.007	0.014	0.10	1.0	10	100
h (nm)	2.9	2.9	3.2	3.6	3.9	3.9	3.9

value for the medium dielectric constant; in any case, the volume fraction of the GNRs in solution is sufficiently small that it does not effect the medium's dielectric constant.

We found that the transient absorption signals measured at the peak of the plasmon absorption (Figure 4a) can be used to extract both the thermal conductivity and heat capacity of the CTAB layers surrounding the GNRs. The rapid decay during the first 10 ps is due to electron−phonon coupling, and is followed by acoustic vibrations (the wiggles in Figure 4) which decay by ~500 ps.[5] These acoustic vibrations have been studied before, and comprise radial and longitudinal modes of the GNRs.[46]

Data were analyzed using a heat conduction model developed by A. Schmidt and co-workers.[24] We combine the interfacial thermal conductances of particle/surface and surface layer/solvent interfaces to report an effective thermal conductivity that considers a series of "resistors": the thermal resistance to heat flow from the gold to the organic, in series with heat flow from the organic to the water. The calculated thicknesses (h) of the CTAB bilayer in different samples, using eqs 5−9, are displayed in Table 1. For GNRs in CTAB solutions above the critical micelle concentration, we used a thickness of 3.9 nm. Since the absorption spectra and transient absorption of the 10 mM CTAB and 100 mM CTAB solutions are similar to that of GNRs in 1 mM CTAB solution, it implies that the CTAB bilayer structure for GNRs in >1 mM CTAB solution is constant.

A typical fit of the transient absorption data to the model is shown in Figure 4b; the fit is constrained to delay times between 30 ps and 2 ns. We treated the thermal conductivity (Λ) and volumetric heat capacity
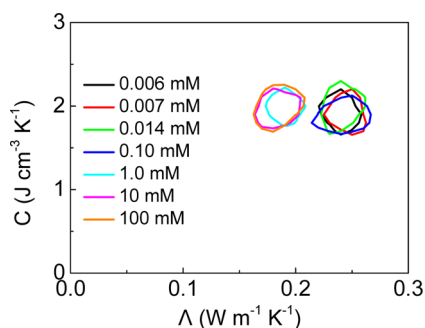
Figure 5. Data fitting for thermal conductivity and volumetric heat capacity of CTAB-coated GNRs in CTAB solutions. The contour edge indicates the Λ-C combinations that have a deviation between the fit and the data that is twice the minimum deviation.

(C) of the CTAB bilayer as free parameters in the fit. The deviation (D) between the fit and the data was calculated using eq 10.

$$ D = \frac{\sum_{i=1}^{n} \left(\frac{|abs_{Fit}|_i - |abs_{Data}|_i}{|abs_{Data}|_i} \right)^2}{n} \quad (10) $$

where $|abs_{Fit}|$ and $|abs_{Data}|$ are the absolute absorbance of the fit and data at a certain delay time, respectively; n is the number of points. A contour of constant deviation between the fit and the data for this two-dimensional parameter space is plotted in Figure 5. This contour is drawn at the points where the deviations are twice the minimum deviation (D = 10^{-3}) between the data and the fit.

The thermal conductivity (Λ) of the CTAB bilayer is centered at ~0.24 W m^{-1} K^{-1} for samples at CTAB concentrations <1 mM, which decreases to ~0.18 W m^{-1} K^{-1} for samples at CTAB concentration >1 mM. The data further suggest that a full CTAB bilayer has a thermal conductivity more dominated by the organic alkyl chain than water, as thermal conductivities for alkanes at 20 °C are 0.11−0.14 W m^{-1} K^{-1} while that of water is 0.61 W m^{-1} K^{-1}.[23,47] The volumetric heat capacity of the CTAB bilayer is constant and centered at 2.0 J cm^{-3} K^{-1}, which is similar to the values reported for many polymers.[28]

The surface charge of CTAB-coated GNRs is positive in water.[48] Polyelectrolyte layer-by-layer coating is an effective way to increase the thickness of the surface layers on GNRs and also to convert positively charged nanorods into negatively charged ones and vice versa.[48] For GNRs with polyelectrolyte coatings, the longitudinal plasmon peak shifts after each coating step due to the change in the refractive index of the surrounding media (Figure 6a); here, poly(acrylic acid) (PAA) is the anionic polyelectrolyte, and poly-(allylamine hydrochloride (PAH)) is the cationic polyelectrolyte, which are added in succession to the surface of GNRs. The first PAA layer coating blue-shifts the plasmon peak ~8 nm. This phenomenon can be
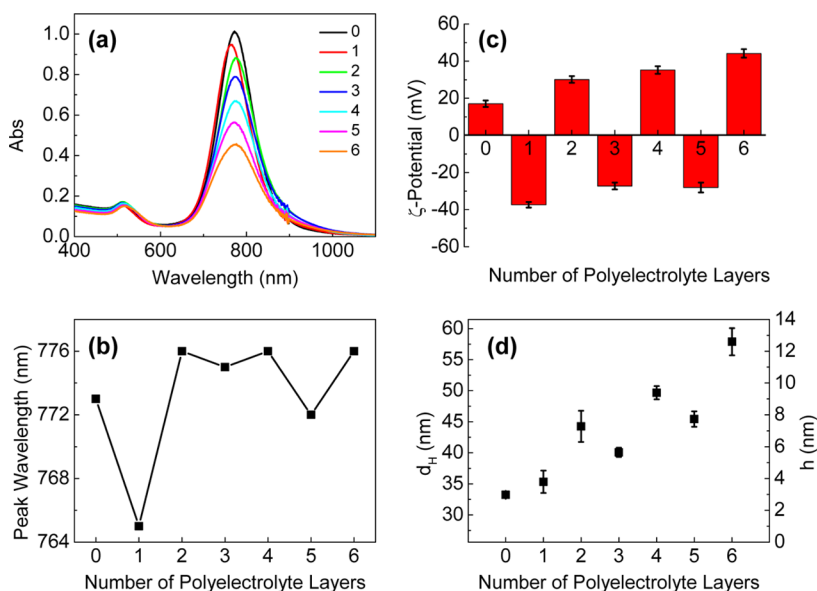
Figure 6. (a) UV−vis absorption spectra of GNRs with different numbers of PAA and PAH alternating polyelectrolyte coating layers (1, 3, 5 = PAA; 2, 4, 6 = PAH). The number of polyelectrolyte layer 0 refers to the as-prepared GNR pellets dispersed directly in water; (b) longitudinal plasmon peak maxima for GNRs as a function of polyelectrolyte layers; (c) ζ-potential of GNRs as a function of polyelectrolye layers; (d) effective hydrodynamic diameters (d_H) of GNRs with polyelectrolyte layers measured by dynamic light scattering; and equivalent thicknesses (h) of polyelectrolyte layers calculated from eqs 5−9.

TABLE 2. Thickness of Polyelectrolyte Layers (PEL) on Wrapped GNRs

| no. of PEL	0	1	2	3	4	5	6
h (nm)	2.9	3.8	7.2	5.6	9.4	7.7	12.6

explained by considering that the surrounding environment change from organic-like to water-like, as hydrophilic PAA molecules replace part of the CTAB bilayer and bring associated water molecules near the GNR surface. As additional polyelectrolyte layers are deposited, the plasmon peak maximum shifts slightly, in an alternating fashion, for each layer (Figure 6b), which we hypothesize is due to the differential hydration of the PAA layers compared to the PAH layers. ζ-Potential measurements confirm the alternating surface charge upon successive rounds of PAA or PAH coating (Figure 6c).

Dynamic light scattering measurements show an increasing hydrodynamic diameter of the particles after the polyelectrolyte coatings, as expected, although the PAA/PAH alternating behavior in the shift of the plasmon band is recapitulated in an alternating trend in overall effective size (Figure 6d). Whether this means that polyelectrolyte layers are being released for the odd-number layers, or multilayers are added for the even-number layers, is not clear from this data alone. Nonetheless, the same approaches for transient absorption measurements and data analysis can be applied to these samples as they were to the CTAB-coated samples.

The calculated thickness for the polyelectrolyte layers is shown in Table 2. The increasing thickness of

PAA-terminated (layers 1, 3, 5) coating layers measured by DLS is not reflected in the degree of red-shifting of the plasmon absorption peak that would be expected if the index of refraction of the coating is constant. In other words, as the coating layer increases, the coating layers are apparently becoming less dense and perhaps more hydrated. The PAH-terminated (layers 2, 4, 6) coating layers with the increasing layer thickness have the same plasmon absorption peak position. This also implies that as the number of coating layers increases, the density decreases. As these DLS measurements are made over long time scales compared to the transient optical experiments, the thickness estimate of the layers necessarily assumes a constant value for the medium dielectric constant; in any case, the volume fraction of the GNRs in solution is sufficiently small that it does not affect the medium's dielectric constant.

Transient absorption data were acquired at the wavelength of peak absorption of the polyelectrolyte-wrapped GNRs. The transient absorption changes of samples with PAH as the outer layer (layers 2, 4, 6) are significantly slower than samples with PAA as the outer layer (layers 1, 3, 5; Figure 7a). To fit the transient absorption data, all the polyelectrolyte layers and the original CTAB layer are considered as one surface layer with uniform thermal properties. A typical fit of the transient absorption data to the model is shown in Figure 7b. Both the thermal conductivity (Λ) and volumetric heat capacity (C) are varied to fit the transient absorption curves. Contours of constant deviation between the fit and the data for this two-dimensional parameter space are plotted in Figure 8.
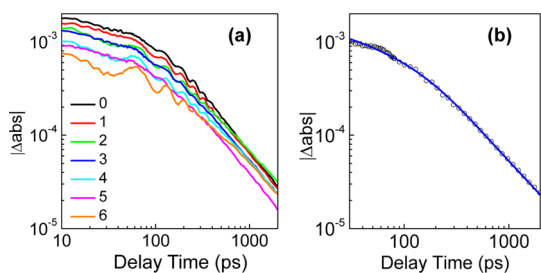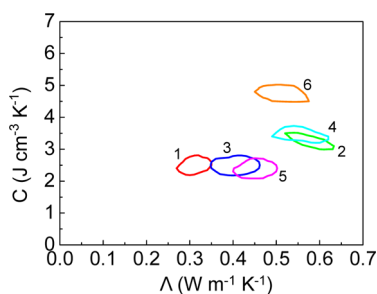
Figure 7. (a) Transient absorption of GNRs with different numbers of polyelectrolyte coating layers. (b) (Circle) raw data of GNRs with 3 layers of polyelectrolyte coatings from pump−probe measurement; (line) fitting for thermal conductivity of 0.38 W m^{-1} K^{-1}, and volumetric heat capacity of 2.5 J cm^{-3} K^{-1} for polyelectrolyte layers.

Figure 8. Data fitting for thermal conductivity and volumetric heat capacity of multilayer polyelectrolyte-coated GNRs in aqueous solutions. Layers 1, 3, and 5 are PAA, and layers 2, 4, and 6 are PAH. The contour indicates the Λ-C combinations that have twice as much as the minimum deviation between the raw data and fitted data.

This contour is drawn at the points where the deviations are twice the minimum deviation between the raw data and the fitted data.

For PAA-terminated samples (layers 1, 3, 5), the Λ values increase from 0.32 to 0.45 W m^{-1} K^{-1} as the number of coating layers increases; C values range between 2.2 and 2.8 J cm^{-3} K^{-1}. The increased Λ and C values compared to the CTAB-only coated GNRs can be explained by possible water penetration when the polyelectrolytes are present. For PAH-terminated samples (layers 2, 4, 6), Λ values decrease slightly from 0.58 to 0.53 W m^{-1} K^{-1}, while C values increase from ~3.2 to ~4.8 J cm^{-3} K^{-1} as the number of coating layers increases. The larger numbers compared to CTAB-only and PAA-terminated GNRs suggest that even more water is present near the GNR surface for PAH-terminated GNRs.

Periodic changes in water content with alternative anionic and cationic polyelectrolyte multilayer coatings have been widely observed.[49−53] Neutron reflectivity studies of multilayers of polystyrene sulfonate (PSS) and PAH on silicon surfaces suggest that these polyelectrolyte multilayer films are heavily hydrated; water occupies >40% of the volume within the films.[49] In the PSS/PAH study, the data suggested that the water content varied periodically with the nature of the layers (PSS was more hydrated than PAH).[49] The swelling behavior of layer-by-layer assemblies of PSS/PAH was investigated.[50] A pronounced "odd-even effect" in the thickness and refractive index of the swollen layers depending on the outmost layer type was observed. They concluded that water is pressed out of the multilayers when PAH is adsorbed onto the PSS layer and more water penetrates into the multilayer after the next adsorption of PSS layer.[50] A similar "odd−even effect" in the thickness[54] and Young's modulus[55] for PAA/PAH multilayers have been reported, in which the PAA-terminated multilayers have relatively smaller thickness[54] and higher Young's modulus[55] than the PAH-terminated multilayers. Our data suggest that a similar situation is present in the PAA/PAH multilayers on GNRs, in that the apparent water content varies periodically with the nature of the wrapping layers, and therefore affects thermal conductivity and heat capacity of the layers.

CONCLUSIONS

Transient absorption spectra of gold nanorods with rationally tuned surface coatings have been examined for different surface treatments, in order to analyze the thermal conductivity and heat capacity of the coatings. The quaternary ammonium surfactant CTAB forms a bilayer on the gold nanorods, with CTAB above the critical micelle concentration fixing the structure of the bilayer and the thermal properties. Dynamic light scattering can be used to measure the thickness of the surface layer with high precision. Polyelectrolyte multilayer coatings on top of the CTAB alter the apparent hydrophobic organic environment around the GNRs; polyelectrolyte and water penetration results in the increased thermal conductivity and heat capacity for the surface layers. The thermal conductivity and heat capacities measured in a transient absorption experiment can be used to infer the physical and chemical nature of species within ~10 nm of the surface of gold nanorods.

EXPERIMENTAL SECTION

Materials. Hydrogen tetrachloroaurate (III) hydrate (HAuCl$_4$· 3H$_2$O, 99.999%), sodium borohydride (NaBH$_4$, 99.99%), silver nitrate (AgNO$_3$, >99.0%), (poly(acrylic acid) sodium salt), M.W. $\approx$ 15 000 (35 wt % solution in H$_2$O) (PAA), and polyallyamine hydrochloride, M.W. $\approx$ 15 000 (PAH) were obtained from Aldrich. Cetyltrimethylammonium bromide (CTAB, >99%) and

ascorbic acid (C$_6$H$_8$O$_6$, >99.0%) were purchased from Sigma Chemical. Sodium chloride (>99.0%) was obtained from Fischer Chemicals. All of these reagents were used without any further purification. All solutions were prepared using Barnstead E-Pure 18 MΩ water.

Synthesis of Gold Nanorods. Gold nanorods with aspect ratios of ~3.8 were synthesized using a seed-mediated silver-assisted

method.[30] At first, gold seeds with diameters of ~2−4 nm were synthesized by adding 0.6 mL of 0.01 M ice-cold $NaBH_4$ solution into a mixture of 0.25 mL of 0.01 M $HAuCl_4$ aqueous solution and 9.75 mL of 0.1 M cetyltrimethylammonium bromide (CTAB) aqueous solution, followed by vigorous stirring for 10 min. The prepared brownish gold seed solution stood for 30 min before use. GNR growth solutions were prepared by mixing 0.5 mL of 0.01 M $HAuCl_4$ solution, 9.5 mL of 0.1 M CTAB solution, and 0.1 mL of 0.01 M $AgNO_3$ solution. Then 0.055 mL of 0.1 M ascorbic acid solution as a reducing agent was added into the growth solution, and 0.012 mL of gold seed solution was added and the solution was allowed to stand overnight. The as-made GNR solution was purified twice by centrifugation at 11000 rpm for 20 min to remove excess surfactants and other reactants. The synthesis could be scaled up to 200 mL.

Preparation of Gold Nanorods in CTAB Solutions. GNRs in different concentrations of CTAB solutions were prepared by dispersing 0.05 mL of the twice-purified GNR pellet into 1.5 mL deionized water or into 1.5 mL 0.001, 0.01, 0.1, 1, 10, 100 mM CTAB solutions.

Preparation of Gold Nanorods Coated with Polyelectrolyte Layers. GNRs coated with different layers of polyelectrolytes were prepared by the layer-by-layer adsorption approach.[48] Solutions of 1 mL of 0.01 M NaCl solution and 2 mL of of 10 mg mL^{-1} poly(acrylic acid sodium salt) (PAA) or polyallylamine hydrochloride (PAH) (M.W. ≈ 15 000) were added into 10 mL of 0.5 nM GNR solutions and shaken for 2 h to coat the GNR surface with polyelectrolyte multilayers. After each coating step, samples were diluted to 20 mL with deionized water, purified by centrifugation at 8000 rpm for 20 min (Thermo Scientific Sorvall Legend X1 centrifuge in a "swinging bucket" orientation) and redispersed in deionized water.

Characterization of Gold Nanorod Aqueous Solutions. The final GNR samples were characterized with UV−vis absorption spectrometer, transmission electron microscopy, ζ-potential and dynamic light scattering measurements. Absorption spectra of the diluted samples with GNR concentration of ~0.15 nM were taken on a Cary 500 scan UV−vis−NIR spectrophotometer. ζ-Potential and dynamic light scattering measurements of samples with GNR concentrations of ~1 nM were taken on a Brookhaven ZetaPALS instrument. Transmission electron microscope images were taken on a JEOL 2100 Cryo TEM microscope at 200 kV accelerating voltage. TEM grids were prepared by drop-casting 15 μL of ~1 nM purified GNRs on a holey carbon TEM grid (Pacific Grid-Tech).

Transient Absorption Measurement. A mode-locked Ti:sapphire laser that produces a series of <0.5 ps pulses at a repetition rate of 80 MHz was used for transmission measurement. The relative optical path lengths of pump beam and probe beam are adjusted *via* a mechanical delay stage. A 5X microscope objective lens was used to focus the pump and probe beams on the sample with the $1/e^2$ laser spot radius of 10.3 μm. Flat-sided capillary tubes with the inner dimension of $0.1 \times 2\ mm^2$ were used as fluid cell for GNR suspensions. The pump and probe beam powers were set at ~1.5 mW, and the wavelengths could be adjusted from 730 to 830 nm. Sharp-edged optical filters (790 LP, 785 ± 1.5 BP, 780 SP, 770 SP from Omega Filters) were used to separate the pump and probe wavelengths as needed. The differences in transmitted probe intensity caused by the pump pulse appear at the f = 9.8 MHz modulation frequency of the pump beam and were extracted with lock-in detection.[21−23] Two quarter-wave plates were fixed before the objective lens and photodetector individually to change the linear polarized beam to circular polarized beam and back. Transient absorption measurements to determine the thermal decay of multilayer-coated GNRs was taken with both the pump and probe wavelengths tuned to the absorption peaks of the GNR samples.

Conflict of Interest: The authors declare no competing financial interest.

REFERENCES AND NOTES

1. Murphy, C. J.; Sau, T. K.; Gole, A. M.; Orendorff, C. J.; Gao, J.; Gou, L.; Hunyadi, S. E.; Li, T. Anisotropic Metal Nanoparticles: Synthesis, Assembly, and Optical Applications. *J. Phys. Chem. B* **2005**, *109*, 13857−13870.

2. Murphy, C. J.; Thompson, L. B.; Chernak, D. J.; Yang, J. A.; Sivapalan, S. T.; Boulos, S. P.; Huang, J.; Alkilany, A. M.; Sisco, P. N. Gold Nanorod Crystal Growth: From Seed-Mediated Synthesis to Nanoscale Sculpting. *Curr. Opin. Colloid Interface Sci.* **2011**, *16*, 128−134.

3. Huang, X.; Neretina, S.; El-Sayed, M. A.; Huang, X.; Neretina, S.; El-Sayed, M. A. Gold Nanorods: From Synthesis and Properties to Biological and Biomedical Applications. *Adv. Mater.* **2009**, *21*, 4880−4910.

4. Ekici, O.; Harrison, R. K.; Durr, N. J.; Eversole, D. S.; Lee, M.; Ben-Yakar, A. Thermal Analysis of Gold Nanorods Heated with Femtosecond Laser Pulses. *J. Phys. D: Appl. Phys.* **2008**, *41*, 185501.

5. Hartland, G. V. Optical Studies of Dynamics in Noble Metal Nanostructures. *Chem. Rev.* **2011**, *111*, 3858−3887.

6. Norman, R. S.; Stone, J. W.; Gole, A.; Murphy, C. J.; Sabo-Attwood, T. L. Targeted Photothermal Lysis of the Pathogenic Bacteria, Pseudomonas Aeruginosa, with Gold Nanorods. *Nano Lett.* **2008**, *8*, 302−306.

7. Bartczak, D.; Muskens, O. L.; Millar, T. M.; Sanchez-Elsner, T.; Kanaras, A. G. Laser-Induced Damage and Recovery of Plasmonically Targeted Human Endothelial Cells. *Nano Lett.* **2011**, *11*, 1358−1363.

8. Huang, Y.-F.; Sefah, K.; Bamrungsap, S.; Chang, H.-T.; Tan, W. Selective Photothermal Therapy for Mixed Cancer Cells Using Aptamer-Conjugated Nanorods. *Langmuir* **2008**, *24*, 11860−11865.

9. Huang, J.; Jackson, K. S.; Murphy, C. J. Polyelectrolyte Wrapping Layers Control Rates of Photothermal Molecular Release from Gold Nanorods. *Nano Lett.* **2012**, *12*, 2982−2987.

10. Kuo, T.-R.; Hovhannisyan, V. A.; Chao, Y.-C.; Chao, S.-L.; Chiang, S.-J.; Lin, S.-J.; Dong, C.-Y.; Chen, C.-C. Multiple Release Kinetics of Targeted Drug from Gold Nanorod Embedded Polyelectrolyte Conjugates Induced by Near-Infrared Laser Irradiation. *J. Am. Chem. Soc.* **2010**, *132*, 14163−14171.

11. Wijaya, A.; Schaffer, S. B.; Pallares, I. G.; Hamad-Schifferli, K. Selective Release of Multiple DNA Oligonucleotides from Gold Nanorods. *ACS Nano* **2008**, *3*, 80−86.

12. Huschka, R.; Zuloaga, J.; Knight, M. W.; Brown, L. V.; Nordlander, P.; Halas, N. J. Light-Induced Release of DNA from Gold Nanoparticles: Nanoshells and Nanorods. *J. Am. Chem. Soc.* **2011**, *133*, 12247−12255.

13. Cahill, D. G.; Ford, W. K.; Goodson, K. E.; Mahan, G. D.; Majumdar, A.; Maris, H. J. Merlin, R.; Phillpot, S. R. Nanoscale Thermal Transport. *J. Appl. Phys.* **2003**, *93*, 793−818.

14. Shakouri, A. Nanoscale Thermal Transport and Microrefrigerators on a Chip. *Proc. IEEE* **2006**, *94*, 1613−1638.

15. Adleman, J. R.; Boyd, D. A.; Goodwin, D. G.; Psaltis, D. Heterogenous Catalysis Mediated by Plasmon Heating. *Nano Lett.* **2009**, *9*, 4417−4423.

16. Christopher, P.; Xin, H.; Linic, S. Visible-Light-Enhanced Catalytic Oxidation Reactions on Plasmonic Silver Nanostructures. *Nat. Chem.* **2011**, *3*, 467−472.

17. Fasciani, C.; Alejo, C. J. B.; Grenier, M.; Netto-Ferreira, J. C.; Scaiano, J. C. High-Temperature Organic Reactions at Room Temperature Using Plasmon Excitation: Decomposition of Dicumyl Peroxide. *Org. Lett.* **2011**, *13*, 204−207.

18. Maity, S.; Downen, L. N.; Bochinski, J. R.; Clarke, L. I. Embedded Metal Nanoparticles as Localized Heat Sources: An Alternative Processing Approach for Complex Polymeric Materials. *Polymer* **2011**, *52*, 1674−1685.

19. Wang, Z.; Cahill, D. G.; Carter, J. A.; Koh, Y. K.; Lagutchev, A.; Seong, N.-H.; Dlott, D. D. Ultrafast Dynamics of Heat Flow Across Molecules. *Chem. Phys.* **2008**, *350*, 31−44.

20. Chen, S.; Lee, I. Y. S.; Tolbert, W. A.; Wen, X.; Dlott, D. D. Applications of Ultrafast Temperature Jump Spectroscopy to Condensed Phase Molecular Dynamics. *J. Phys. Chem.* **1992**, *96*, 7178−7186.

21. Wilson, O.; Hu, X.; Cahill, D.; Braun, P. Colloidal Metal Particles as Probes of Nanoscale Thermal Transport in Fluids. *Phys. Rev. B* **2002**, *66*, 224310.

22. Ge, Z.; Cahill, D. G.; Braun, P. V. AuPd Metal Nanoparticles as Probes of Nanoscale Thermal Transport in Aqueous Solution. *J. Phys. Chem. B* **2004**, *108*, 18870–18875.

23. Ge, Z.; Kang, Y.; Taton, T. A.; Braun, P. V.; Cahill, D. G. Thermal Transport in Au-Core Polymer—Shell Nanoparticles. *Nano Lett.* **2005**, *5*, 531–535.

24. Schmidt, A. J.; Alper, J. D.; Chiesa, M.; Chen, G.; Das, S. K.; Hamad-Schifferli, K. Probing the Gold Nanorod—Ligand—Solvent Interface by Plasmonic Absorption and Thermal Decay. *J. Phys. Chem. C* **2008**, *112*, 13320–13323.

25. Alper, J.; Hamad-Schifferli, K. Effect of Ligands on Thermal Dissipation from Gold Nanorods. *Langmuir* **2010**, *26*, 3786–3789.

26. Juvé, V.; Scardamaglia, M.; Maioli, P.; Crut, A.; Merabia, S.; Joly, L.; Fatti, N.; Del; Vallée, F. Cooling Dynamics and Thermal Interface Resistance of Glass-Embedded Metal Nanoparticles. *Phys. Rev. B* **2009**, *80*, 195406.

27. Hu, M.; Wang, X.; Hartland, G. V.; Salgueiriño-Maceira, V.; Liz-Marzán, L. M. Heat Dissipation in Gold—Silica Core—Shell Nanoparticles. *Chem. Phys. Lett.* **2003**, *372*, 767–772.

28. Mark, J. E. *Physical Properties of Polymers Handbook*; Springer: New York, 2006, pp 145—163.

29. Pelton, M.; Liu, M.; Park, S.; Scherer, N. F.; Guyot-Sionnest, P. Ultrafast Resonant Optical Scattering from Single Gold Nanorods: Large Nonlinearities and Plasmon Saturation. *Phys. Rev. B* **2006**, *73*, 155419.

30. Sau, T. K.; Murphy, C. J. Seeded High Yield Synthesis of Short Au Nanorods in Aqueous Solution. *Langmuir* **2004**, *20*, 6414–6420.

31. Murphy, C. J.; Thompson, L. B.; Alkilany, A. M.; Sisco, P. N.; Boulos, S. P.; Sivapalan, S. T.; Yang, J. A.; Chernak, D. J.; Huang, J. The Many Faces of Gold Nanorods. *J. Phys. Chem. Lett.* **2010**, *1*, 2867–2875.

32. Petrova, H.; Perez Juste, J.; Pastoriza-Santos, I.; Hartland, G. V.; Liz-Marzán, L. M.; Mulvaney, P. On the Temperature Stability of Gold Nanorods: Comparison between Thermal and Ultrafast Laser-Induced Heating. *Phys. Chem. Chem. Phys.* **2006**, *8*, 814–821.

33. Kang, K.; Koh, Y. K.; Chiritescu, C.; Zheng, X.; Cahill, D. G. Two-Tint Pump-Probe Measurements Using a Femtosecond Laser Oscillator and Sharp-Edged Optical Filters. *Rev. Sci. Instrum.* **2008**, *79*, 114901–114904.

34. Sönnichsen, C.; Franzl, T.; Wilk, T.; Plessen, G.; von; Feldmann, J.; Wilson, O.; Mulvaney, P. Drastic Reduction of Plasmon Damping in Gold Nanorods. *Phys. Rev. Lett.* **2002**, *88*, 077402.

35. Winsemius, P. *Temperature Dependence of the Optical Properties of Au and Ag.* Ph.D. Dissertation, Rijks-Universiteit te Leiden, 1973.

36. Cardinal, M. F.; Mongin, D.; Crut, A.; Maioli, P.; Rodríguez-González, B.; Pérez-Juste, J.; Liz-Marzán, L. M.; Fatti, N.; Del; Vallée, F. Acoustic Vibrations in Bimetallic Au@Pd Core—Shell Nanorods. *J. Phys. Chem. Lett.* **2012**, *3*, 613–619.

37. Baida, H.; Mongin, D.; Christofilos, D.; Bachelier, G.; Crut, A.; Maioli, P.; Fatti, N.; Del; Vallée, F. Ultrafast Nonlinear Optical Response of a Single Gold Nanorod near Its Surface Plasmon Resonance. *Phys. Rev. Lett.* **2011**, *107*, 057402.

38. Link, S.; El-Sayed, M. A. Spectral Properties and Relaxation Dynamics of Surface Plasmon Electronic Oscillations in Gold and Silver Nanodots and Nanorods. *J. Phys. Chem. B* **1999**, *103*, 8410–8426.

39. Uematsu, M.; Frank, E. U. Static Dielectric Constant of Water and Steam. *J. Phys. Chem. Ref. Data* **1980**, *9*, 1291–1306.

40. Link, S.; Mohamed, M. B.; El-Sayed, M. A. Simulation of the Optical Absorption Spectra of Gold Nanorods as a Function of Their Aspect Ratio and the Effect of the Medium Dielectric Constant. *J. Phys. Chem. B* **1999**, *103*, 3073–3077.

41. Alkilany, A. M.; Nagaria, P. K.; Wyatt, M. D.; Murphy, C. J. Cation Exchange on the Surface of Gold Nanorods with a Polymerizable Surfactant: Polymerization, Stability, and Toxicity Evaluation. *Langmuir* **2010**, *26*, 9328–9333.

42. Ming, T.; Kou, X.; Chen, H.; Wang, T.; Tam, H.-L.; Cheah, K.-W.; Chen, J.-Y.; Wang, J. Ordered Gold Nanostructure Assemblies Formed By Droplet Evaporation. *Angew. Chem., Int. Ed.* **2008**, *47*, 9685–9690.

43. Hamon, C.; Postic, M.; Mazari, E.; Bizien, T.; Dupuis, C.; Even-Hernandez, P.; Jimenez, A.; Courbin, L.; Gosse, C.; Artzner, F.; *et al.* Three-Dimensional Self-Assembling of Gold Nanorods with Controlled Macroscopic Shape and Local Smectic B Order. *ACS Nano* **2012**, *6*, 4137–4146.

44. Rodríguez-Fernández, J.; Pérez-Juste, J.; Liz-Marzán, L. M.; Lang, P. R. Dynamic Light Scattering of Short Au Rods with Low Aspect Ratios. *J. Phys. Chem. C* **2007**, *111*, 5020–5025.

45. Ortega, A.; García de la Torre, J. Hydrodynamic Properties of Rodlike and Disklike Particles in Dilute Solution. *J. Chem. Phys.* **2003**, *119*, 9914–9919.

46. Zijlstra, P.; Tchebotareva, A. L.; Chon, J. W. M.; Gu, M.; Orrit, M. Acoustic Oscillations and Elastic Moduli of Single Gold Nanorods. *Nano Lett.* **2008**, *8*, 3493–3497.

47. Dashora, P.; Gupta, G. On the Temperature Dependence of the Thermal Conductivity of Linear Amorphous Polymers. *Polymer* **1996**, *37*, 231–234.

48. Gole, A.; Murphy, C. J. Polyelectrolyte-Coated Gold Nanorods: Synthesis, Characterization and Immobilization. *Chem. Mater.* **2005**, *17*, 1325–1330.

49. Lösche, M.; Schmitt, J.; Decher, G.; Bouwman, W. G.; Kjaer, K. Detailed Structure of Molecularly Thin Polyelectrolyte Multilayer Films on Solid Substrates as Revealed by Neutron Reflectometry. *Macromolecules* **1998**, *31*, 8893–8906.

50. Wong, J. E.; Rehfeldt, F.; Hänni, P.; Tanaka, M.; Klitzing, R. v. Swelling Behavior of Polyelectrolyte Multilayers in Saturated Water Vapor. *Macromolecules* **2004**, *37*, 7285–7289.

51. McCormick, M.; Smith, R. N.; Graf, R.; Barrett, C. J.; Reven, L.; Spiess, H. W. NMR Studies of the Effect of Adsorbed Water on Polyelectrolyte Multilayer Films in the Solid State. *Macromolecules* **2003**, *36*, 3616–3625.

52. Schlenoff, J. B.; Rmaile, A. H.; Bucur, C. B. Hydration Contributions to Association in Polyelectrolyte Multilayers and Complexes: Visualizing Hydrophobicity. *J. Am. Chem. Soc.* **2008**, *130*, 13589–13597.

53. Schwarz, B.; Schönhoff, M. Surface Potential Driven Swelling of Polyelectrolyte Multilayers. *Langmuir* **2002**, *18*, 2964–2966.

54. Liu, X.; Goli, K. K.; Genzer, J.; Rojas, O. J. Multilayers of Weak Polyelectrolytes of Low and High Molecular Mass Assembled on Polypropylene and Self-Assembled Hydrophobic Surfaces. *Langmuir* **2011**, *27*, 4541–4550.

55. Lehaf, A. M.; Moussallem, M. D.; Schlenoff, J. B. Correlating the Compliance and Permeability of Photo-Cross-Linked Polyelectrolyte Multilayers. *Langmuir* **2011**, *27*, 4756–4763.